JOURNAL OF GUIDANCE, CONTROL, AND DYNAMICS
Vol. 22, No. 1, January–February 1999

Full Envelope Missile Autopilot Design Using Gain Scheduled Robust Control

Harald Buschek*
BGT Bodenseewerk Gerätetechnik GmbH, 88641 Überlingen, Germany

The challenge to cope with highly nonlinear and rapidly time-varying dynamics will be a prevailing factor when designing autopilots for next-generation agile missiles. Robust control techniques are employed to design lateral and roll controllers for an agile skid-to-turn missile. Uncertainty models for variations in the aerodynamic coefficients and in the first flexible-body mode have been introduced. The controllers are scheduled as a function of dynamic pressure using a novel conditioning/blending technique to achieve full flight envelope control capability. A high-fidelity nonlinear six-degree-of-freedom simulation accounting for structural vibrations and various noise effects is used to verify the approach in a practical setting. A sequence of lateral acceleration commands and a realistic engagement scenario demonstrate the performance and robustness properties of the designed autopilots. The applicability of linear robust control techniques to nonlinear dynamic systems is illustrated in an authentic environment employing the challenging example of a highly maneuverable missile.

I. Introduction

AUTOPILOT design for future missile systems will be dominated by the requirement of ultimate agility in the entire flight envelope of the missile. Critical issues for next-generation autopilots will not only be a fast response to the required acceleration demands or to provide extreme maneuverability while maintaining stability, but also to guarantee robustness over a wide range of mission profiles at all altitudes. Accelerating and decelerating flight conditions, varying mass and inertia properties, perturbations in the thrust profile, or uncertain effectiveness of the control surfaces are among the effects leading to a highly nonlinear behavior of the missile dynamics in the considered flight envelope.

Classical control techniques have dominated missile autopilot design over the past several decades. Most guided missile systems employ acceleration and rate feedback together with proportional and integral control to stabilize the missile and to track the guidance command signals.[1] The gains of these autopilots are obtained in a variety of linearized flight conditions and have to be scheduled by appropriate algorithms to account for the changing environment.

The development of robust control techniques in the 1980s has revolutionized flight control system design considerably. Methods such as H_∞ design and μ-synthesis provide the means to design multivariable controllers that satisfy performance specifications and simultaneously guarantee stability when the system deviates from its nominal design condition and/or is subject to exogenous disturbances.[2–4] Robust autopilots for the linearized missile dynamics in the pitch plane have been designed in Refs. 5–7. An H_∞ flight controller for the coupled pitch, yaw, and roll dynamics is illustrated in Ref. 8. H_∞ control is also employed in Ref. 9 for a bank-to-turn autopilot considering the effects of flexible-body dynamics and noise.

Autopilots that are designed using robust control techniques are capable of covering a significant fraction of the flight envelope. Nevertheless, one single robust controller will most likely not suffice to satisfy all performance and robustness requirements throughout the full envelope. This will particularly be true in the case of agile missiles with rapidly changing dynamics. In general, gain scheduling as it is commonly used for conventional proportional/integral controllers cannot directly be applied to robust controllers. These controllers may not have the explicit structure required to interpolate the individual gains with respect to changing flight conditions. A simple approach to adjust a robust controller to a changing environment is given in Ref. 10 by scheduling the input signal levels to the controller as a function of Mach number. A separation of a designed pitch controller into a pair of single input/single output transfer functions describing a linearized acceleration error controller and a linearized pitch rate controller is employed in Ref. 11. The poles and zeros of the resulting transfer functions are interpolated with respect to changing angles of attack and Mach numbers.

The transition from linear time-invariant systems to linear parameter-varying (LPV) systems represents another approach to extend the autopilot design envelope. In Ref. 12, an LPV formulation is used in conjunction with multiple μ-synthesis controllers for both the pitch and the roll/yaw channels. The missile dynamics are considered in the endgame phase of the flight only, assuming constant altitude and velocity. An LPV formulation of the short-period dynamics is used in Ref. 13. A linear matrix inequality approach is chosen to design a self-scheduled H_∞ controller depending on real-time measurements of angle of attack, velocity, and altitude. If sufficient system information and computing power are available, the state-dependent Riccati equation (SDRE) method from Ref. 14 can be used. The nonlinear dynamics are parametrized to obtain a linear structure having state-dependent coefficients. The resulting SDREs of the corresponding H_2 problem are then solved at each time step yielding a nonlinear H_2 design. A direct application of H_∞ control techniques to nonlinear systems is presented in Refs. 15 and 16, which involves the replacement of the Riccati equation with the so-called Hamilton–Jacobi–Isaacs equation.

Another approach to design autopilots for agile missiles is to apply feedback linearization techniques to the nonlinear missile dynamics. However, difficulties arise with the nonminimum phase characteristic of tail-controlled missiles, when normal acceleration is commanded. A two-timescale separation technique and a redefinition of the output are used in Ref. 17 to alleviate this problem for a pitch autopilot. The singular perturbation technique, together with a partial linearization, is employed in Ref. 18 to pursue the same goal. A feedback linearization autopilot using an adaptive neural network structure is presented in Ref. 19 and is applied to a bank-to-turn missile.

In this paper, a full envelope skid-to-turn autopilot for an agile air-to-air missile is designed using μ-synthesis methods. The controllers are scheduled as a function of dynamic pressure employing a conditioning/blending technique. Implementation issues of the linear designs in a nonlinear environment are discussed. A sequence of lateral acceleration step commands and a realistic engagement scenario are evaluated in a detailed nonlinear six-degree-of-freedom simulation. The results illustrate the applicability of the selected approach.

Presented as Paper 97-3763 at the AIAA Guidance, Navigation, and Control Conference, New Orleans, LA, Aug. 11–13, 1997; received Oct. 23, 1997; revision received May 11, 1998; accepted for publication May 29, 1998.

*Research Engineer, System Design, Missile Division, P.O. Box 101155. E-mail: Harald.Buschek@bgt.de. Member AIAA.

II. Missile Model

A tail-controlled, agile air-to-air missile with an axisymmetric configuration is used. To apply linear control techniques, the nonlinear missile dynamics are linearized and decoupled into three simplified sets of dynamic equations for the pitching, yawing, and rolling motion. Because of the axisymmetric property of the missile, a skid-to-turn steering policy can be employed. This steering policy has no preferred maneuver plane and selects both the longitudinal and the lateral plane to command the required accelerations. Accordingly, there is no clear distinction between longitudinal and lateral-directional control as is the case with bank-to-turn missiles. Employing decoupled dynamics, this fact is naturally accommodated by using one autopilot that is identical for the longitudinal and the lateral plane (lateral autopilot) and a separate roll autopilot that provides attitude stabilization.

The linearized equations of motion of the lateral missile dynamics including the effects of thrust vector control (TVC) are

$$\begin{aligned}\dot{\beta} &= (Y_\beta/V_0)\beta - r + [(Y_\zeta/V_0) + c_{\text{th}}(T/mV_0)]\zeta \\ \dot{r} &= N_\beta\beta + N_r r + [N_\zeta - c_{\text{th}}(l_{\text{th}}T/I_z)]\zeta\end{aligned} \tag{1}$$

where β is sideslip angle, r yaw rate, and ζ rudder deflection. The derivatives $Y_\beta, \ldots, N_\zeta$ are a function of the present flight condition, sideslip angle, and rudder deflection. V_0 is the velocity at the linearized flight condition, m is mass, and I_z is the moment of inertia. The influence of thrust vector control is represented by the thrust T, the distance l_{th} between the center of gravity and the nozzle, and the factor c_{th} relating the fin deflection angle to the actual thrust vector deflection.

The lateral acceleration at the center of gravity is given by

$$\begin{aligned}a_{y,\text{cg}} &= V_0(\dot{\beta} + r) \\ &= Y_\beta\beta + [Y_\zeta + c_{\text{th}}(T/m)]\zeta\end{aligned} \tag{2}$$

and the corresponding acceleration at the location of the accelerometer is

$$\begin{aligned}a_{y,\text{acc}} &= a_{\text{cg}} + l_{\text{acc}}\dot{r} \\ &= (Y_\beta + l_{\text{acc}}N_\beta)\beta + l_{\text{acc}}N_r r \\ &\quad + \{Y_\zeta + l_{\text{acc}}N_\zeta + c_{\text{th}}[(T/m) - l_{\text{acc}}(l_{\text{th}}T/m)]\}\zeta\end{aligned} \tag{3}$$

where l_{acc} represents the distance from the accelerometer to the center of gravity. The time dependency of variables such as mass, moment of inertia, etc., is neglected in the linear models.

Although the system dynamics have been linearized at certain flight conditions corresponding to specific Mach numbers and altitudes, there exists an additional dependence of the aerodynamic derivatives on sideslip angle and control deflection. The resulting variation of the linearized system dynamics due to a change in these variables is accounted for by uncertainty models in the aerodynamic derivatives Y_β, Y_ζ, N_β, and N_ζ. To simplify the design procedure, variations in thrust are neglected, and a representative average value is assumed.

Structural vibrations due to aeroelastic effects corrupt measured accelerations and body rates. These vibrations may lead to induced oscillations and even rigid–elastic body mode coupling resulting in possible performance degradations of the missile. This phenomenon is also taken into account in the autopilot design procedure. Because treating the fully coupled rigid–elastic equations of motion would be beyond the scope of this study, a simplified model has been developed to represent the impact of flexible-body effects on the measurement signals (see Ref. 20). The following transfer function characterizes the additional acceleration measured by the accelerometer due to aeroelastic vibrations of the structure excited by fin deflections to control the missile:

$$a_i(x_{\text{acc}}, s) = s^2\Phi_i(x_{\text{acc}})\frac{\Phi_i(x_{\text{Fin}})\bar{q}SC_{Y\zeta} + c_{\text{th}}\Phi_i(x_{\text{TVC}})T}{\left(s^2 + 2\zeta_i\omega_i s + \omega_i^2\right)M_i}\zeta(s) \tag{4}$$

Accordingly, the additional body rate measured by the gyros is

$$r_i(x_{\text{gyro}}, s) = s\left[\frac{\mathrm{d}\Phi_i(x)}{\mathrm{d}x}\right]_{x = x_{\text{gyro}}}\frac{\Phi_i(x_{\text{Fin}})\bar{q}SC_{Y\zeta} + c_{\text{th}}\Phi_i(x_{\text{TVC}})T}{\left(s^2 + 2\zeta_i\omega_i s + \omega_i^2\right)M_i}\zeta(s) \tag{5}$$

where $\bar{q}$ is dynamic pressure and S is the reference area. The frequencies of the elastic modes ω_i, mode shapes Φ_i, and the modal masses M_i can be determined by a finite element analysis of the missile structure. The mode shapes are evaluated at the corresponding locations of the sensors, fins, and nozzle, respectively. It is important to realize that the aeroelastic properties of the structure are changing while the motor is burning and propellant is consumed. To a certain extent, this is accounted for by modeling the variations of the natural frequencies ω_i as uncertainties to cover the body bending characteristics from launch to motor burnout.

For roll autopilot design, the linearized roll dynamics of the missile including TVC effects are given by

$$\dot{p} = L_p p + [L_\xi - c_{\text{th}}l_{\text{th},p}(T/I_x)]\xi, \qquad \dot{\Phi} = p \tag{6}$$

where p is roll rate, Φ roll angle, and ξ aileron deflection. As with the lateral dynamics, uncertainty models for the uncertain aerodynamic coefficients L_p and L_ξ are introduced to achieve the desired robustness characteristics. Flexible-body characteristics do not need to be modeled in the roll channel because the frequencies of torsional structural vibrations are considerably higher than roll autopilot bandwidth.

III. Controller Design Using μ-Synthesis

A. Lateral Controller

As described in Sec. II, both rigid-body and flexible-body dynamics are included in the lateral controller design procedure. It is sufficient to include only the first elastic mode because it is the one that has the most crucial impact on the rigid-body behavior.

To improve the dynamic representation of the missile, a model of the actuation system is included in the design. The actuator is modeled as a second-order system with a bandwidth of 30 Hz and damping of 0.7.

The interconnection structure for controller design is shown in Fig. 1. The design is carried out as an acceleration command tracking system. The additional accelerations and body rates originating in the flexible-body dynamics are superposed on the corresponding signals of the rigid-body dynamics. The uncertainty in the aerodynamic coefficients is represented by the structured uncertainty block

$$\Delta = \begin{bmatrix}\delta_\beta & \\ & \delta_\zeta\end{bmatrix} \tag{7}$$

where δ_β and δ_ζ account for the uncertainty in Y_β, N_β, and Y_ζ, N_ζ, respectively.

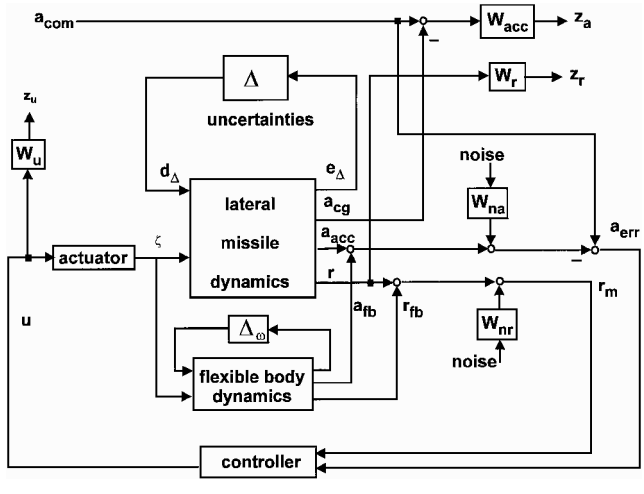

Fig. 1 Generalized plant for lateral controller design.

The uncertain frequency of the first body bending mode is modeled in a simplified fashion according to Ref. 21. Only variations in the ω^2 term in Eqs. (4) and (5) are considered. Treating the real perturbation in the natural frequency as complex in the framework of μ-synthesis serves to introduce uncertainty also in the $2\zeta\omega$ term in Eqs. (4) and (5) even though it is not explicitly considered.[21] The uncertainty is shown by Δ_ω in Fig. 1.

Weighted measurement noise corrupts the feedback channels

$$W_{na} = 0.001, \qquad W_{nr} = 0.005 \tag{8}$$

In addition to the robustness requirements introduced into the design by the uncertainties and external disturbances, performance specifications are imposed by individual weighting functions. The weighting W_{acc} on the error signal between commanded and achieved acceleration defines the desired speed of response and steady-state error of the resulting closed-loop system. The weighting on yaw rate, W_r, introduces damping into the design whereas the weighting on the control, W_u, is important to limit controller bandwidth. This constrains the control deflections to the limits of the actuator and reduces the feedthrough of measurement noise to the actuation unit. This is a crucial issue in a realistic controller design because noisy fin deflection command signals lead to an increased power consumption in the actuation system. On the other hand, if controller bandwidth is restricted too much the overall missile performance will degrade due to slow autopilot responses. Therefore, an optimal tradeoff between robustness properties, noise rejection, and performance specifications needs to be found. In practice, an appropriate selection of the weighting functions is achieved iteratively by alternate controller design and simulation steps. As an example, the optimal weights for the present design in the medium dynamic pressure region were determined to be

$$W_{\text{acc}} = \frac{100[(1/300)s + 1]}{(1/0.03)s + 1} \tag{9}$$

$$W_r = 5 \tag{10}$$

$$W_u = \frac{0.001[(1/0.007)s + 1]}{(1/1400)s + 1} \tag{11}$$

Using μ-synthesis, three controllers have been designed at representative flight conditions covering the full envelope of the missile. A standard order-reduction technique using a balanced realization[22] was employed to reduce the dimension of the inherently high-order μ controllers. All controllers could be reduced to seventh-order without sacrificing the robust performance levels of the full-order designs.

To illustrate some representative properties of the robust controllers, the frequency response plot of one of the controllers is shown in Fig. 2. The transfer function from the measured acceleration error to the control signal exhibits two characteristic features:

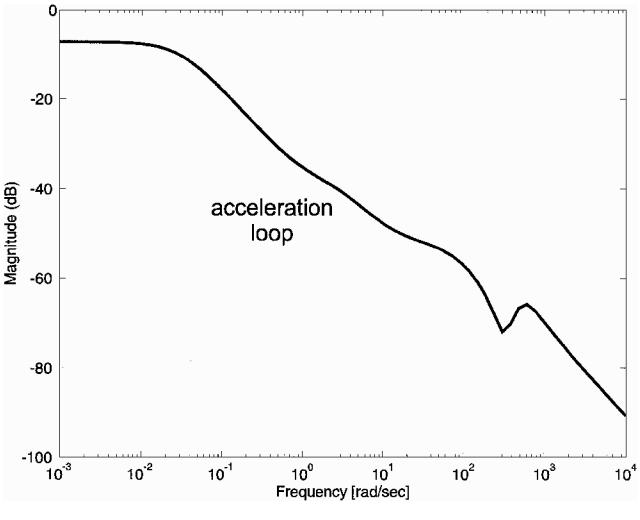

Fig. 2 Frequency response plot of lateral controller.

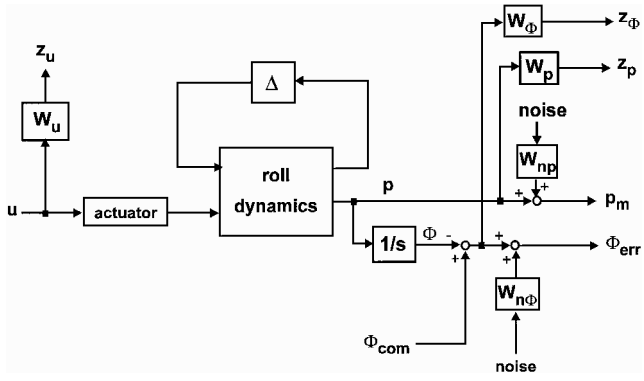

Fig. 3 Generalized plant for roll controller design.

a strong rolloff at higher frequencies to reduce the impact of high-frequency measurement noise in the acceleration loop and an additional indentation at the first body bending frequency to damp the flexible-body mode. Because the frequency of the first mode has been considered uncertain in the design, the indentation is not distinct but broader to capture the effect of the varying frequency during motor burning. This indentation demonstrates how the controller performs an implicit notch filtering of the body bending dynamics. Hence, extra notch filters are rendered obsolete.

B. Roll Controller

The selected skid-to-turn steering policy requires the roll autopilot to perform an attitude stabilization in the maneuver plane and to provide adequate roll damping. Accordingly, the roll controller is designed as a roll angle command tracking system as shown in Fig. 3.

Similar to the lateral autopilot, a robust control design approach is pursued. The error signal between commanded and achieved roll angle Φ_{err} is fed back to the controller together with the measured roll rate p_m for additional roll damping. Weighting functions on Φ_{err}, p_m, and control u determine the characteristics of the resulting closed-loop system

$$W_\Phi = \frac{125[(1/600)s + 1]}{(1/0.24)s + 1} \tag{12}$$

$$W_p = 0.01 \tag{13}$$

$$W_u = \frac{0.0001[(1/0.01)s + 1]}{(1/4000)s + 1} \tag{14}$$

Uncertainty models for the uncertain aerodynamic coefficients L_p and L_ξ are introduced to achieve the desired robustness characteristics

$$\Delta = \begin{bmatrix} \delta_p & \\ & \delta_\xi \end{bmatrix} \tag{15}$$

The actuator model from the lateral design is included. Weighted noise disturbances corrupting the measurements are characterized by

$$W_{n\phi} = 0.001, \qquad W_{np} = 0.1 \tag{16}$$

Again, three different robust roll controllers have been designed for the full envelope of the missile. As in the lateral case, the controllers were reduced to seventh-order without a loss in robust performance.

Various analyses regarding the performance and robustness of the designed lateral and roll controllers have been carried out using linear techniques and simulations. However, a detailed description of these linear results is omitted in favor of an in-depth discussion on implementation and simulation of the linear robust controllers in a highly nonlinear, realistic environment.

IV. Autopilot Implementation Issues

A. Controller Scheduling

As described in Sec. III, three controllers have been designed for the lateral and the roll autopilot, respectively. Each controller covers

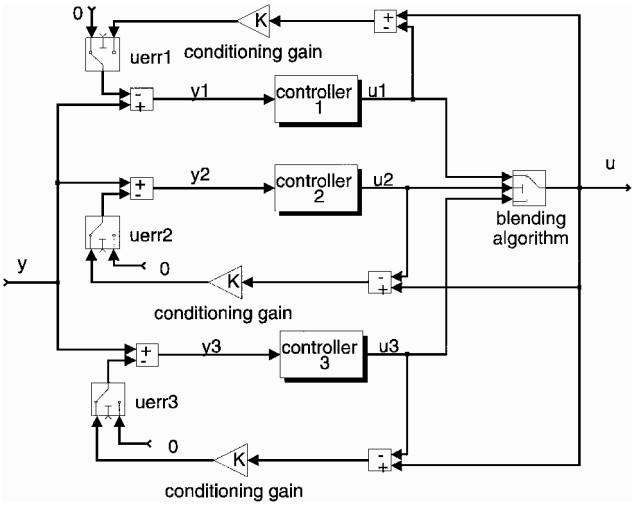

Fig. 4 Controller conditioning/blending scheme.

a certain dynamic pressure region and is used for all velocities, altitudes, angles of attack, sideslip angles, etc., in this region. The controllers are implemented using a combined conditioning/blending scheme, which is derived from the so-called "high-gain antiwindup approach" in Ref. 23. This technique achieves a smooth transition between controllers by ensuring that the states of the next controller to be switched in are consistent with the current system states. The setup is shown in Fig. 4. Here, controller 1 is on-line while the off-line controllers 2 and 3 are being conditioned. The conditioning is performed using the error signal between the outputs of the off-line controllers and the output of active controller 1

$$u_{\text{err}\,2,3} = K(u - u_{2,3}) \tag{17}$$

K is a conditioning gain to allow for an improved adaptation to active controller 1. In the case of the lateral autopilot, the measurement vector that is fed to the controllers is given by (see Fig. 1)

$$\boldsymbol{y} = \begin{bmatrix} a_{\text{err}} \\ r_m \end{bmatrix} \tag{18}$$

The driving element for the controllers is the acceleration error a_{err}, whereas yaw rate r_m is used mainly for damping purposes. The idea of conditioning is to artificially increase the acceleration error for the off-line controllers whenever their respective control outputs are too small in comparison with the output of the on-line controller and to reduce the acceleration error whenever their control outputs are too high. With the present missile dynamics, the control deflections are defined such that a positive rudder deflection results in a negative lateral acceleration. Therefore, the error in the control output enters the measurement vector with a negative sign:

$$\boldsymbol{y}_{2,3} = \begin{bmatrix} a_{\text{err}} - u_{\text{err}\,2,3} \\ r_m \end{bmatrix} \tag{19}$$

When transferring between controllers, a blending approach is used to avoid the typical bumps when conditioning is not fully completed and controllers are simply switched instantaneously. The outputs of the corresponding controllers are selected as a function of changing dynamic pressure. As already mentioned, each controller covers a certain dynamic pressure region. These regions are selected such that they overlap for a certain amount (see Fig. 5). When dynamic pressure enters these overlapping sectors, the outputs of the two corresponding controllers are blended by linear interpolation:

$$\begin{aligned} &\bar{q} < \bar{q}_l: && u = u_1 \\ &\bar{q}_l \le \bar{q} \le \bar{q}_u: && u = \left(1 - \frac{\bar{q} - \bar{q}_l}{\bar{q}_u - \bar{q}_l}\right) u_1 + \frac{\bar{q} - \bar{q}_l}{\bar{q}_u - \bar{q}_l} u_2 \\ &\bar{q}_u < \bar{q}: && u = u_2 \end{aligned} \tag{20}$$

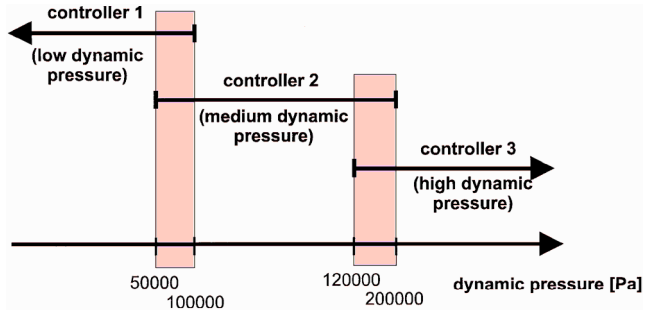

Fig. 5 Dynamic pressure ranges for blending the lateral controllers.

where $\bar{q}_l$ and $\bar{q}_u$ are the lower and upper bounds of the overlapping dynamic pressure sector, respectively. While the outputs are blended, conditioning is performed for both controllers simultaneously. Because both controllers yield a robustly stable closed-loop system in their respective dynamic pressure regions, blending their outputs in the overlapping sector will also result in a stable system for most practical cases. Nevertheless, additional simulations are still required to properly adjust the conditioning gain and the bounds of the overlapping sector to ensure that a smooth transition from one controller to the other is achieved.

In the case of the lateral autopilot, blending between the low and the medium dynamic pressure controllers is performed between 50 and 100 kPa, and the medium and high dynamic pressure controllers are blended between 120 and 200 kPa. The roll controllers are scheduled in a similar fashion, with slightly different dynamic pressure regions.

B. Implementation

The three lateral controllers together with the conditioning/blending logic constitute the lateral autopilot. As mentioned earlier, this lateral autopilot is implemented twice: once to control the yaw dynamics and once to control the pitch dynamics. Accordingly, the roll autopilot consists of the three scheduled roll controllers.

The feedback signals that need to be provided are accelerations and body angular rates, which are commonly available through sensors. If dynamic pressure for controller scheduling is not directly measured, it can be estimated utilizing initial information supplied by the launching aircraft.

Presently, all controllers have been reduced to seventh-order. However, there is no requirement that all controllers be of the same dimension. The conditioning/blending technique is capable of dealing with controllers of arbitrary dimensions.

V. Nonlinear Evaluation

A. Six-Degree-of-Freedom Simulation

To verify the performance and robustness characteristics of the designed autopilots in an authentic nonlinear environment, a high-fidelity six-degree-of-freedom (6-DOF) simulation is employed. The standard equations of motion for an axisymmetric configuration in body axes are given by

$$\begin{aligned} \dot{u} &= vr - wq + (1/m)(F_x + T_x) + g_x \\ \dot{v} &= wp - ur + (1/m)(F_y + T_y) + g_y \\ \dot{w} &= uq - vp + (1/m)(F_z + T_z) + g_z \\ \dot{p} &= (1/I_x)(L + L_T) \\ \dot{q} &= (1/I_y)[M + M_T - pr(I_x - I_z)] \\ \dot{r} &= (1/I_z)[N + N_T - pq(I_y - I_x)] \end{aligned} \tag{21}$$

where (u, v, w) are the velocity components and (p, q, r) the corresponding angular rates. (F_x, F_y, F_z) represent the aerodynamic forces, (L, M, N) the aerodynamic moments, (T_x, T_y, T_z) the thrust forces, and (L_T, M_T, N_T) the thrust moments. In Eq. (21) (g_x, g_y, g_z) are the gravitational accelerations. Mass m and moments

of inertia are time varying and change according to the burned propellant.

The aerodynamic forces and moments are determined by

$$F_x = \bar{q}Sc_x, \qquad F_y = \bar{q}Sc_y, \qquad F_z = \bar{q}Sc_z$$
$$L = \bar{q}Sd\left[c_L + c_{Lp}p(d/V)\right]$$
$$M = \bar{q}Sd\left[c_M + \left(c_{Mq}q + c_{M\dot{\alpha}}\dot{\alpha}\right)(d/V)\right] \tag{22}$$
$$N = \bar{q}Sd\left[c_N + \left(c_{Nr}r + c_{N\dot{\beta}}\dot{\beta}\right)(d/V)\right]$$

where $\bar{q}$ is dynamic pressure, S the reference area, d the reference length, and V the total velocity of the missile. The aerodynamic coefficients are extracted from tables and take into account the current values of angle of attack, sideslip angle, roll angle, control surface deflection, and center of gravity position. The thrust forces and moments are calculated by a representative propulsion system and TVC model.

The effects of flexible-body dynamics are implemented using the transfer functions in Eqs. (4) and (5) with all variables being updated as the simulation proceeds. Accordingly, not only the natural frequency changes as accounted for in the controller design, but mode shapes and modal mass are also functions of time. Actuator models including rate and deflection limits, as well as sensor models for the accelerometers and gyros including measurement noise, are incorporated. Other noise models account for motor vibrations and aerodynamic noise deteriorating the quality of the feedback signals.

B. Acceleration Step Commands

To carry out an initial investigation on autopilot performance and on the applicability of the implemented scheduling technique, a sequence of positive and negative 10-g lateral acceleration step commands is imposed on the missile. Figure 6 shows the missile's response where time has been normalized with respect to motor burnout time t_{bo}. A slight tendency to overshoot and minor steady-state errors are detectable. Nevertheless, the overall response is fast and provides adequate tracking of the acceleration command. The nonminimum phase behavior of a tail-controlled missile is evident in the initial accelerations going in the opposite direction of each step command. The magnitude is due to the fast response of the autopilot. Dynamic pressure in pascal (1 Pa $= 1.45 \cdot 10^{-4}$ psi) is shown in Fig. 7 and varies from 30 kPa at launch to 360 kPa at motor burnout and back to 50 kPa at the end of the simulation. Accordingly, the lateral autopilot starts with the low dynamic pressure controller and blends to the medium and subsequently to the high dynamic pressure controller before the boost phase terminates. After motor burnout, the procedure is reversed. During the entire simulation, the transition between controllers is smooth and does not exhibit any bumps or oscillations.

The rudder deflections normalized with respect to the fin deflection limit are shown in Fig. 8. The control action is characterized by a spike-shaped deflection to initiate a rapid turn. Lateral acceleration is then maintained by an almost constant rudder deflection. A minor level of noise is visible in the rudder deflections, which is due to the various noise sources corrupting the measurements. The feedback signal, which is provided by the accelerometer, is shown in Fig. 9 illustrating the impact of noise on the quality of the measurements.

During the lateral acceleration commands, a zero roll angle has to be maintained for roll attitude stabilization. The roll angle in Fig. 10 stays in between ± 0.4 deg for most of the maneuver, demonstrating the capability of the roll autopilot.

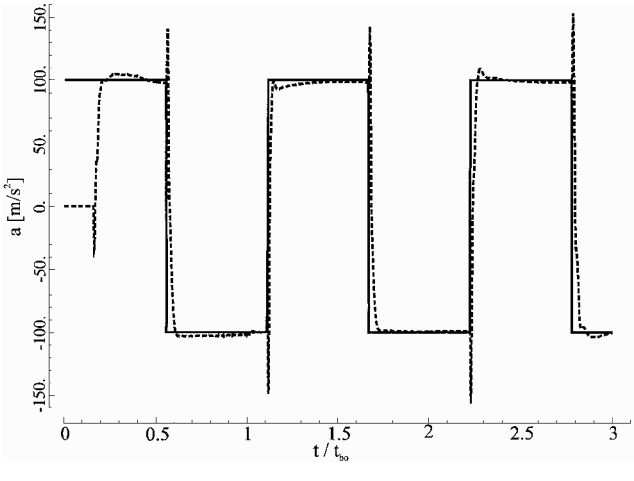

Fig. 6 Lateral accelerations for step commands.

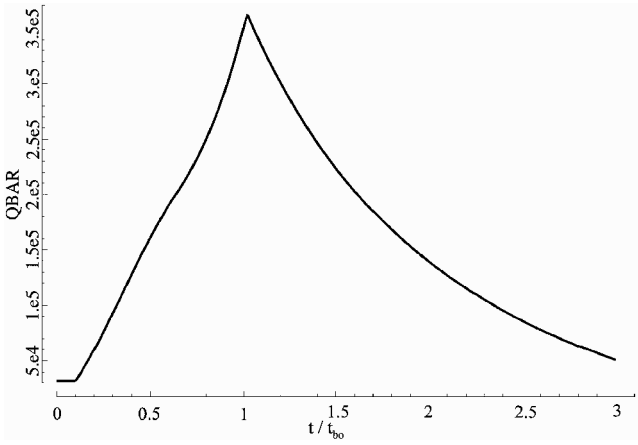

Fig. 7 Dynamic pressure in pascal.

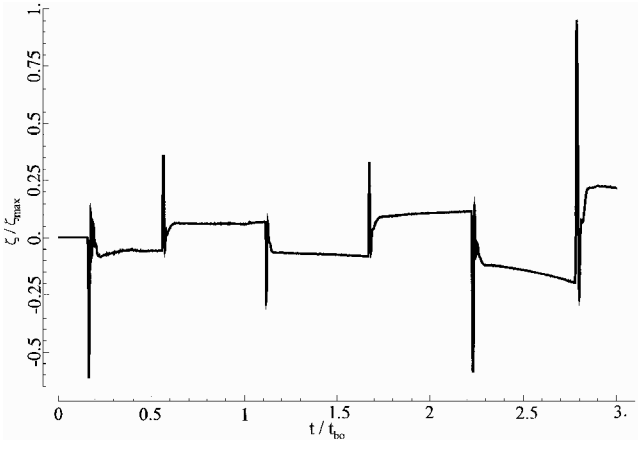

Fig. 8 Normalized rudder deflections.

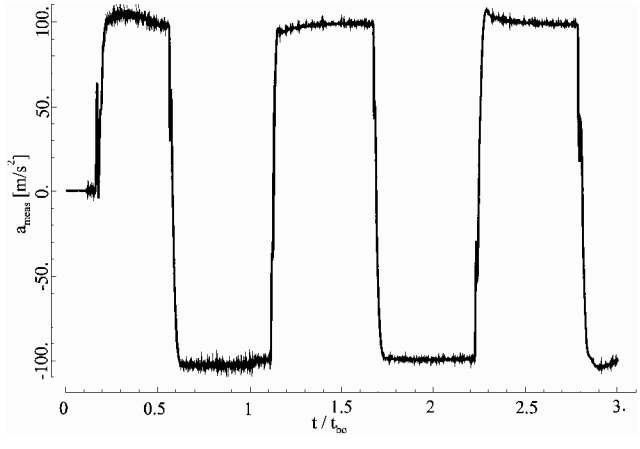

Fig. 9 Measured lateral acceleration.

C. Three-Dimensional Engagement

A realistic engagement scenario is shown in Figs. 11 and 12. The missile is launched horizontally at an altitude h_0. Its position with respect to the target is characterized by an off-tail angle (OTA) of

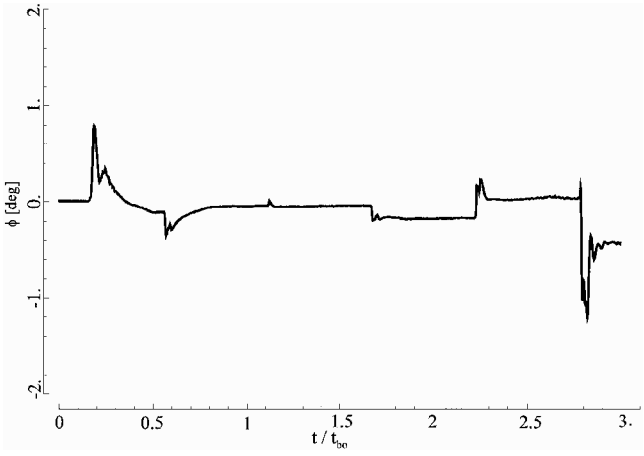

Fig. 10 Roll angle in degrees.

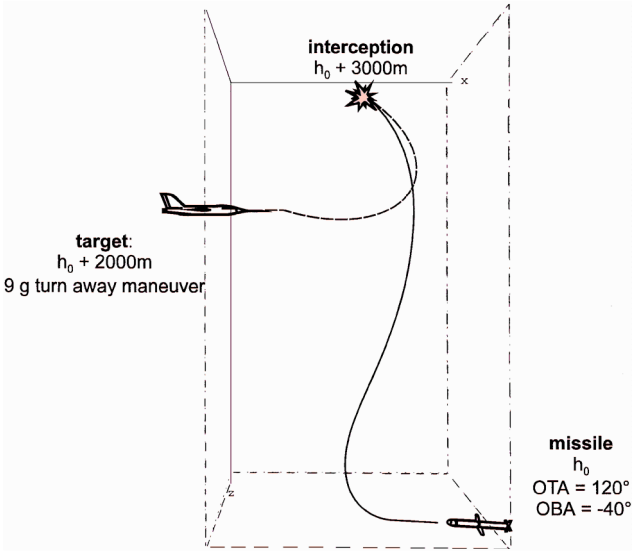

Fig. 11 Engagement scenario, side view.

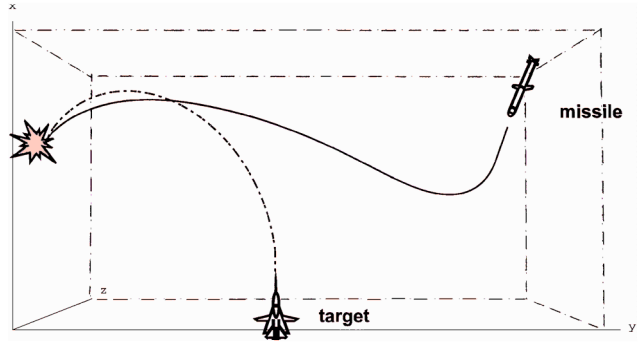

Fig. 12 Engagement scenario, top view.

120 deg and an off-boresight angle (OBA) of −40 deg (lag situation). The target is located at $h_0 + 2000$ m and flies with cospeed. As the missile is launched, the target performs a break-away maneuver with a sustained normal acceleration of $9g$. The missile intercepts the evading target at $h_0 + 3000$ m. In this scenario, all three autopilots are interacting to track the target and to maintain stability. With the present implementation of the skid-to-turn steering policy, normal and lateral acceleration commands are employed to pursue the target while the attitude stabilization requires a zero roll angle.

The normal and lateral acceleration histories are shown in Figs. 13 and 14. Again, time has been normalized with respect to motor burnout time. In both planes, the commands are tracked equally well. Similar to the step command sequence, all three controllers of the lateral autopilot are used, as can be seen from the dynamic

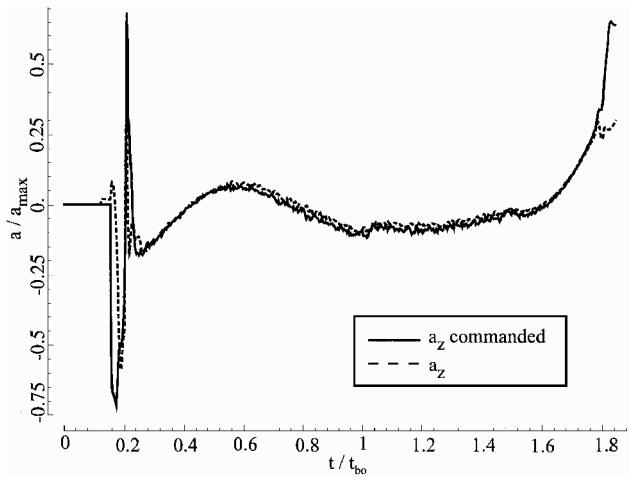

Fig. 13 Normalized normal acceleration.

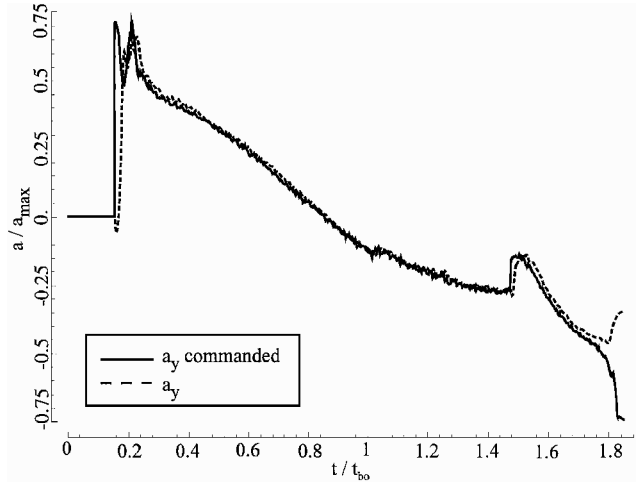

Fig. 14 Normalized lateral acceleration.

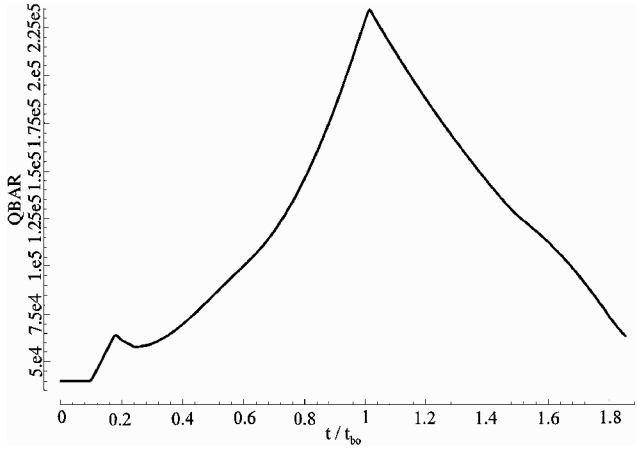

Fig. 15 Dynamic pressure in pascal.

pressure profile in Fig. 15. Again, the scheduling algorithm performs flawlessly. Angle of attack α and sideslip angle β are given in Fig. 16.

Figures 17 and 18 show elevator and rudder deflections η and ζ, respectively. Initial oscillations indicate a certain sensitivity to the relatively large acceleration error immediately after launch. However, the oscillations are also caused by the rapidly changing acceleration commands at the beginning of the maneuver, which have to be tracked by the autopilot. These variations in the command signals are in part due to an initial aerodynamic cross-coupling effect, where the pitch and yaw dynamics couple into the roll dynamics for rapidly increasing α and β, see Figs. 19 and 16. As the missile rolls, the body-fixed normal and lateral accelerations a_z and a_y blend to

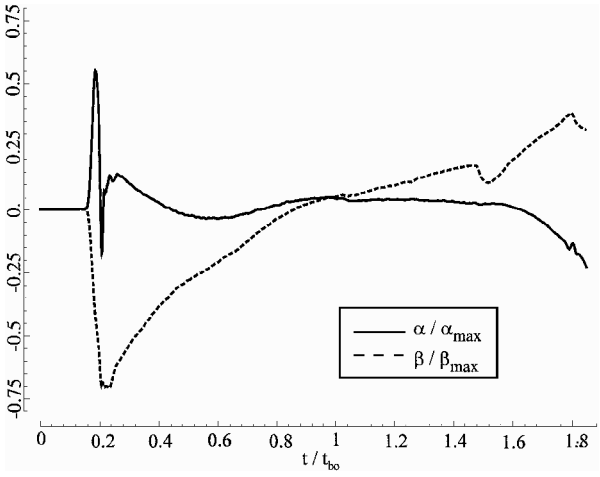

Fig. 16 Normalized angle of attack and sideslip angle.

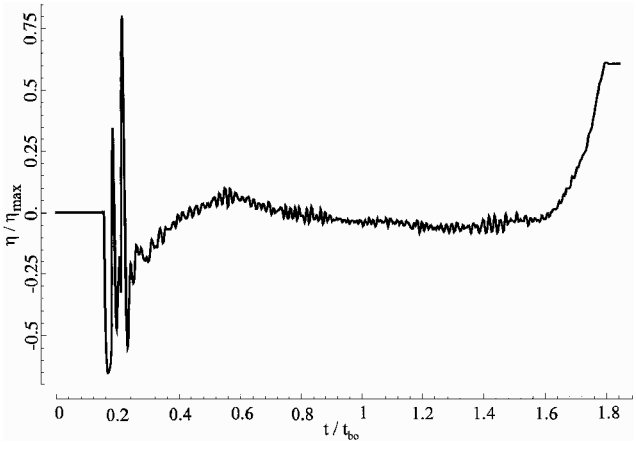

Fig. 17 Normalized elevator deflections.

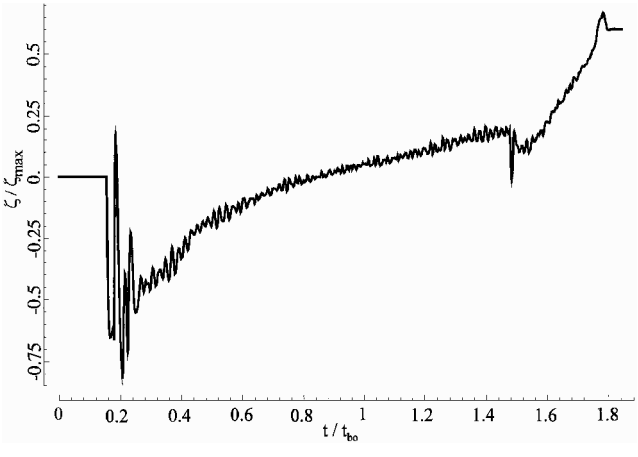

Fig. 18 Normalized rudder deflections.

maintain the pursuit of the target. The aileron deflections of the roll autopilot shown in Fig. 20 counteract this induced rolling motion and are able to stabilize the roll dynamics of the missile. After this initial cross-coupling effect, the maneuver is completed smoothly.

The control histories in Figs. 17, 18, and 20 are characterized by the initial oscillations and a certain sensitivity to noise. Reducing controller bandwidth by adjusting the weights in the linear design procedure can improve both features. However, care must be taken so as not to slow down the controller too much. This could lead to a reduced agility of the missile, resulting in an undesirable loss in performance.

Both the sequence of acceleration steps and the engagement scenario demonstrate the applicability of linear robust controllers on agile missile dynamics in a nonlinear environment. The employed conditioning/blending technique proves to be a feasible tool to schedule the controllers smoothly over the entire flight envelope.

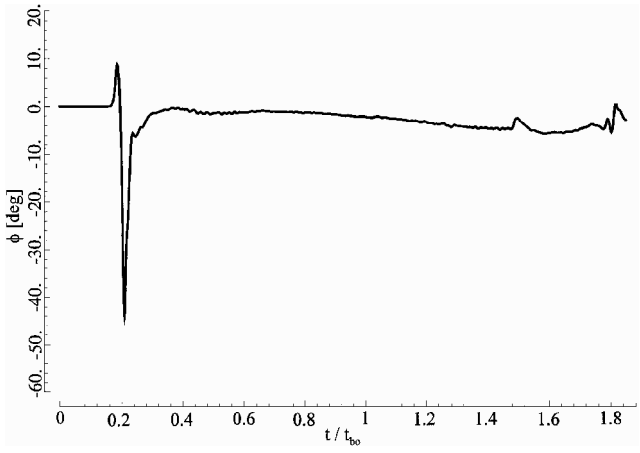

Fig. 19 Roll angle.

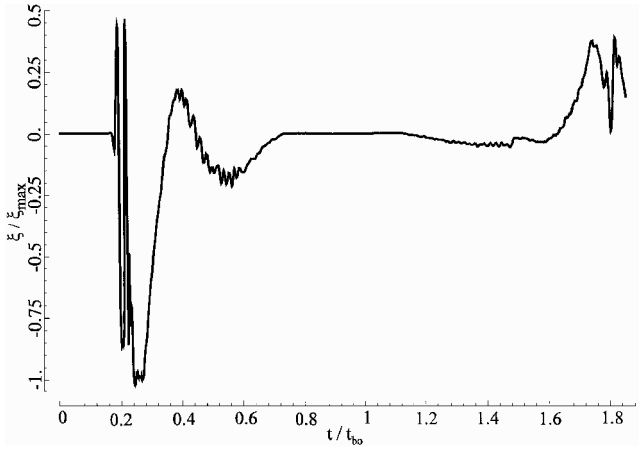

Fig. 20 Normalized aileron deflections.

VI. Conclusions

A full envelope autopilot for an agile air-to-air missile has been designed using robust control techniques. Employing μ-synthesis, three controllers for the lateral dynamics and the roll dynamics have been designed, respectively. A novel conditioning/blending technique is introduced to schedule the controllers over the entire flight envelope as a function of dynamic pressure. The resulting autopilot is evaluated in a sophisticated nonlinear 6-DOF simulation.

The paper illustrates a practical application of advanced control techniques in a realistic environment. The designed linear controllers demonstrate significant robustness and excellent performance characteristics in a highly nonlinear, rapidly time-varying environment. One single controller accounts for all variations in the missile dynamics due to angle-of-attack changes, control surface deflections, and structural vibrations in a considerable section of the entire flight envelope. This illustrates the potential of employing robust control techniques in demanding real-world applications.

The proposed conditioning/blending technique extends the applicability of robust control beyond individual design points. It provides a straightforward methodology to schedule dynamic controllers of arbitrary dimensions. Accordingly, full envelope autopilots can be synthesized utilizing only a small number of controllers. As a result, controller design effort is kept to a minimum while high levels of performance can be achieved over a wide range of operating conditions. The example of a high-agility missile shows that the methodology can be used for challenging practical applications.

References

[1] Nesline, F. W., and Zarchan, P., "Robust Instrumentation Configurations for Homing Missile Flight Control," *Proceedings of the AIAA Guidance,*

Navigation, and Control Conference (Danvers, MA), AIAA, New York, 1980, pp. 209–219.

[2]Doyle, J. C., Glover, K., Khargonekar, P. P., and Francis, B. A., "State-Space Solutions to Standard H_2 and H_∞ Control Problems," *IEEE Transactions on Automatic Control*, Vol. 34, No. 8, 1989, pp. 832–846.

[3]Stein, G., and Doyle, J. C., "Beyond Singular Values and Loop Shapes," *Journal of Guidance, Control, and Dynamics*, Vol. 14, No. 1, 1991, pp. 5–16.

[4]Packard, A., and Doyle, J. C., "The Complex Structured Singular Value," *Automatica*, Vol. 29, No. 1, 1993, pp. 71–109.

[5]Reichert, R. T., "Robust Autopilot Design Using μ-Synthesis," *Proceedings of the American Control Conference* (San Diego, CA), American Automatic Control Council, Evanston, IL, 1990, pp. 2368–2373.

[6]Wise, K. A., Mears, B. C., and Poolla, K., "Missile Autopilot Design Using H_∞ Optimal Control With μ-Synthesis," *Proceedings of the American Control Conference* (San Diego, CA), American Automatic Control Council, Evanston, IL, 1990, pp. 2363–2367.

[7]Yang, S. M., and Huang, N. H., "Application of H_∞ Control to Pitch Autopilot of Missiles," *IEEE Transactions on Aerospace and Electronic Systems*, Vol. 32, No. 1, 1996, pp. 426–433.

[8]Jackson, P., "Applying μ-Synthesis to Missile Autopilot Design," *Proceedings of the 29th IEEE Conference on Decision and Control* (Honolulu, HI), Inst. of Electrical and Electronics Engineers, New York, 1990, pp. 2993–2998.

[9]Lin, C.-F., Cloutier, J. R., and Evers, J. H., "High-Performance, Robust, Bank-to-Turn Missile Autopilot Design," *Journal of Guidance, Control, and Dynamics*, Vol. 18, No. 1, 1995, pp. 46–53.

[10]Balas, G. J., and Packard, A. K., "Design of Robust, Time-Varying Controllers for Missile Autopilots," *Proceedings of the IEEE Conference on Control Applications* (Dayton, OH), Inst. of Electrical and Electronics Engineers, New York, 1992, pp. 104–110.

[11]Nichols, R. A., Reichert, R. T., and Rugh, W. J., "Gain Scheduling for *H*-Infinity Controllers: A Flight Control Example," *IEEE Transactions on Control Systems Technology*, Vol. 1, No. 2, 1993, pp. 69–79.

[12]Carter, L. H., and Shamma, J. S., "Gain-Scheduled Bank-to-Turn Autopilot Design Using Linear Parameter Varying Transformations," *Journal of Guidance, Control, and Dynamics*, Vol. 19, No. 5, 1996, pp. 1056–1063.

[13]Apkarian, P., Biannic, J.-M., and Gahinet, P., "Self-Scheduled H_∞ Control of Missile via Linear Matrix Inequalities," *Journal of Guidance, Control, and Dynamics*, Vol. 18, No. 3, 1995, pp. 532–538.

[14]Mracek, C. P., and Cloutier, J. R., "Missile Longitudinal Autopilot Design Using the State-Dependent Riccati Equation Method," *Proceedings of the International Conference on Nonlinear Problems in Aviation and Aerospace*, Embry–Riddle Aeronautical University, Daytona Beach, FL, 1996, pp. 387–396.

[15]Wise, K. A., and Sedwick, J. L., "Nonlinear H_∞ Optimal Control for Agile Missiles," *Proceedings of the AIAA Guidance, Navigation, and Control Conference* (Baltimore, MD), AIAA, Washington, DC, 1995, pp. 1295–1307 (AIAA Paper 95-3317, Aug. 1995).

[16]Huang, J., and Lin, C.-F., "Numerical Approach to Computing Nonlinear H_∞ Control Laws," *Journal of Guidance, Control, and Dynamics*, Vol. 18, No. 5, 1995, pp. 989–994.

[17]Menon, P. K., and Yousefpor, M., "Design of Nonlinear Autopilots for High Angle of Attack Missiles," AIAA Paper 96-3913, July 1996.

[18]Lee, J.-I., Oh, J.-H., Ha, I.-J., Kim, E.-G., Cho, H.-J., "A New Approach to Autopilot Design for Highly Nonlinear Missiles," AIAA Paper 96-3915, July 1996.

[19]McFarland, M. B., and Calise, A. J., "Neural-Adaptive Nonlinear Autopilot Design for an Agile Anti-Air Missile," AIAA Paper 96-3914, July 1996.

[20]Buschek, H., and Calise, A. J., "Uncertainty Modeling and Fixed-Order Controller Design for a Hypersonic Vehicle Model," *Journal of Guidance, Control, and Dynamics*, Vol. 20, No. 1, 1997, pp. 42–48.

[21]Balas, G. J., and Young, P. M., "Control Design for Variations in Structural Natural Frequencies," *Journal of Guidance, Control, and Dynamics*, Vol. 18, No. 2, 1995, pp. 325–332.

[22]Chiang, R. Y., and Safonov, M. G., "Robust Control Toolbox, User's Guide," MathWorks, Inc., Natick, MA, Aug. 1992.

[23]Hyde, R. A., *H_∞ Aerospace Control Design: A VSTOL Flight Application*, Advances in Industrial Control Series, Springer–Verlag, London, 1995, pp. 63–76.